

# Computation of the response functions of spiral waves in active media

I.V. Biktasheva

*Department of Computer Science, University of Liverpool,  
Ashton Building, Ashton Street, Liverpool L69 3BX, UK*

D. Barkley

*Mathematics Institute, University of Warwick, Coventry CV4 7AL, UK*

V. N. Biktashev and A.J. Foulkes

*Department of Mathematical Sciences, University of Liverpool,  
Mathematics & Oceanography Building, Peach Street, Liverpool, L69 7ZL, UK*

G.V. Bordyugov

*former: Department of Computer Science, University of Liverpool,  
Ashton Building, Ashton Street, Liverpool L69 3BX, UK\**

(Dated: July 5, 2019)

Rotating spiral waves are a form of self-organization observed in spatially extended systems of physical, chemical, and biological nature. A small perturbation causes gradual change in spatial location of spiral's rotation center and frequency, i.e. drift. The Response Functions (RFs) of a spiral wave are the eigenfunctions of the adjoint linearized operator corresponding to the critical eigenvalues  $\lambda = 0, \pm i\omega$ . The RFs describe spirals' sensitivity to small perturbations in the way that a spiral is insensitive to small perturbations where its RFs are close to zero. The velocity of a spiral's drift is proportional to the RFs convolution with the perturbation. We develop regular and generic method of computing the RFs of stationary rotating spirals in the FitzHugh-Nagumo system. We show convergence of the method with respect to the computational parameters, i.e. discretization steps and size of the medium. The obtained Response Functions are localized at the spiral's core.

PACS numbers: 02.60.Cb, 82.40.Bj, 82.40.Ck, 87.10.-e

## I. INTRODUCTION

Autowave vortices, or spiral waves in two-dimensions (2D), are types of self-organization observed in dissipative media of physical [1–4], chemical [5–7], and biological nature [8–13], where wave propagation is supported by a source of energy stored in the medium. The common feature of all these phenomena is that they can be mathematically described, with various degrees of accuracy, by “reaction-diffusion” partial differential equations,

$$\partial_t \mathbf{u} = \mathbf{f}(\mathbf{u}) + \mathbf{D}\nabla^2 \mathbf{u}, \quad \mathbf{u}, \mathbf{f} \in \mathbb{R}^\ell, \quad \mathbf{D} \in \mathbb{R}^{\ell \times \ell}, \quad \ell \geq 2, \quad (1)$$

where  $\mathbf{u}(\vec{r}, t) = (u_1, \dots, u_\ell)^T$  is a column-vector of the reagent concentrations,  $\mathbf{f}(\mathbf{u}) = (f_1, \dots, f_\ell)^T$  of the reaction rates,  $\mathbf{D}$  is the matrix of diffusion coefficients, and  $\vec{r} \in \mathbb{R}^2$  is the vector of coordinates on the plane.

The existence of vortices is not due to singularities in the medium but is determined only by development from initial conditions. A rigidly rotating spiral wave solution to the system (1) has a form

$$\tilde{\mathbf{U}} = \mathbf{U}(\rho(\vec{r} - \vec{R}), \vartheta(\vec{r} - \vec{R}) + \omega t - \Phi), \quad (2)$$

where  $\rho, \vartheta$  are polar coordinates, vector  $\vec{R} = (X, Y)^T$  defines the center of rotation, and  $\Phi$  is initial rotation phase. For a

steady spiral  $\vec{R}$  and  $\Phi$  are constants. The system of reference co-rotating with the spiral's initial phase and angular velocity  $\omega$  around the spiral's center of rotation is called the system of reference of the spiral. In this system of reference,  $\vec{R} = 0$ ,  $\Phi = 0$ , the polar angle  $\theta = \vartheta + \omega t$ , so the spiral wave solution  $\mathbf{U}(\rho, \theta)$  does not depend on time and satisfies the equation

$$\mathbf{f}(\mathbf{U}) - \omega \mathbf{U}_\theta + \mathbf{D}\nabla^2 \mathbf{U} = 0. \quad (3)$$

In this equation, the unknowns are the field  $\mathbf{U}(\rho, \theta)$  and the scalar  $\omega$ .

A slightly perturbed steady spiral wave solution

$$\tilde{\mathbf{U}}(\rho, \theta, t) = \mathbf{U}(\rho, \theta) + \epsilon \mathbf{g}(\rho, \theta, t), \quad \mathbf{g} \in \mathbb{R}^\ell, \quad 0 < \epsilon \ll 1,$$

substituted in (1) yields the evolution equation for the perturbation  $\mathbf{g}$

$$\partial_t \mathbf{g} = \partial_{\mathbf{u}} \mathbf{f}(\mathbf{U}) \mathbf{g} - \omega \partial_\theta \mathbf{g} + \mathbf{D}\nabla^2 \mathbf{g}.$$

Thus, the linear stability spectrum of a steady spiral

$$\mathcal{L}\mathbf{V} = \lambda \mathbf{V} \quad (4)$$

is defined by the linearized operator

$$\mathcal{L} = \mathbf{D}\nabla^2 - \omega \partial_\theta + \partial_{\mathbf{u}} \mathbf{f}(\mathbf{U}). \quad (5)$$

The operator  $\mathcal{L}$  has critical ( $\text{Re}(\lambda) = 0$ ) eigenvalues

$$\lambda_n = in\omega, \quad n = 0, \pm 1, \quad (6)$$

\*Present: The University of Potsdam, Campus Golm, Department of Physics and Astronomy (Haus 28), Karl-Liebknecht-Strasse 24/25, 14476 Potsdam, Germany

which correspond to eigenfunctions related to equivariance of (1) with respect to translations and rotations, *i.e.* “Goldstone modes” (GMs) [14–17]

$$\begin{aligned} \mathbf{V}^{(0)} &= -\partial_\theta \mathbf{U}(\rho, \theta), \\ \mathbf{V}^{(\pm 1)} &= -\frac{1}{2} e^{\mp i\theta} (\partial_\rho \mp i\rho^{-1} \partial_\theta) \mathbf{U}(\rho, \theta). \end{aligned} \quad (7)$$

The stability spectra of steady spiral waves was originally obtained numerically in [16]. Subsequently the spectrum was analysed for infinite and large bounded domains [18–20] with follow on numerical investigations [21] confirming the large domain behavior of the stability spectrum.

In a slightly perturbed problem

$$\partial_t \mathbf{u} = \mathbf{f}(\mathbf{u}) + \mathbf{D}\nabla^2 \mathbf{u} + \epsilon \mathbf{h}, \quad \mathbf{h} \in \mathbb{R}^\ell, \quad 0 < \epsilon \ll 1, \quad (8)$$

where  $\epsilon \mathbf{h}(\mathbf{u}, \vec{r}, t)$  is some small perturbation, spiral waves drift, *i.e.* change rotational phase and/or center location. Then, the center of rotation and the initial phase are no longer constants but become functions of time,  $\vec{R} = \vec{R}(t)$  and  $\Phi = \Phi(t)$ .

In linear approximation, assuming that

$$\dot{\vec{R}}, \dot{\Phi} = \mathcal{O}(\epsilon),$$

the drifting spiral wave solution can be presented as

$$\tilde{\mathbf{U}} = \mathbf{U}(\rho(\vec{r} - \vec{R}(t)), \vartheta(\vec{r} - \vec{R}(t)) + \omega t - \Phi(t)) + \epsilon \mathbf{g}(\vec{r}, t), \quad (9)$$

where  $\epsilon \mathbf{g}(\vec{r}, t)$  is a small perturbation of the steady spiral wave solution  $\mathbf{U}$ .

Then, the solution perturbation  $\mathbf{g}$  in the laboratory frame of reference will satisfy the linearized system

$$\begin{aligned} (\partial_t - \mathbf{D}\nabla^2 - \partial_{\mathbf{u}} \mathbf{f}(\mathbf{U})) \mathbf{g} \\ = \mathbf{h}(\mathbf{u}, \vec{r}, t) - \frac{1}{\epsilon} (\dot{\vec{R}} \cdot \nabla + \dot{\Phi} \partial_\theta) \mathbf{U}. \end{aligned} \quad (10)$$

Solvability condition of the equation (10) for  $\mathbf{g}$ , *i.e.* Fredholm alternative, re-written in the spiral frame of reference, requires that the free term must be orthogonal to the kernel of the adjoint operator to  $\mathcal{L}$  defined in (5). This leads to the system of equations for the drift velocities

$$\dot{\Phi} = \epsilon F_0(\vec{R}, t), \quad \dot{\vec{R}} = \epsilon \vec{F}_1(\vec{R}, t). \quad (11)$$

Thus, the drift velocities  $\dot{\Phi}$  and  $\dot{\vec{R}}$  are determined by the “forces”  $F_0$  and  $\vec{F}_1 = (\text{Re}(F_1), \text{Im}(F_1))^T$  which, after sliding averaging over the spiral wave rotation period, can be expressed [15] as

$$\begin{aligned} F_n(\vec{R}, t) &= e^{in\Phi} \oint_{t-\pi/\omega}^{t+\pi/\omega} \frac{\omega d\tau}{2\pi} e^{-in\omega\tau} \\ &\times \left\langle \mathbf{W}^{(n)} \left( \rho(\vec{r} - \vec{R}), \vartheta(\vec{r} - \vec{R}) + \omega\tau - \Phi \right), \mathbf{h}(\vec{r}, \tau) \right\rangle, \\ n &= 0, \pm 1. \end{aligned} \quad (12)$$

Here  $\langle \cdot, \cdot \rangle$  stands for the scalar product in functional space,

$$\langle \mathbf{w}, \mathbf{v} \rangle = \int_{\mathbb{R}^2} \overline{\mathbf{w}(\vec{r})}^T \mathbf{v}(\vec{r}) d^2 \vec{r}.$$

The kernels  $\mathbf{W}^{(n)}$  of convolution-type integrals in (12) are the spiral wave’s *Response Functions* (RFs), *i.e.* the critical eigenfunctions

$$\mathcal{L}^+ \mathbf{W}^{(n)} = \mu_n \mathbf{W}^{(n)}, \quad (13)$$

where

$$\mu_n = -i\omega n, \quad n = 0, \pm 1, \quad (14)$$

of the adjoint linearized operator:

$$\mathcal{L}^+ = \mathbf{D}\nabla^2 + \omega \partial_\theta + (\partial_{\mathbf{u}} \mathbf{f}(\mathbf{U}))^T, \quad (15)$$

chosen to be biorthogonal

$$\left\langle \mathbf{W}^{(j)}, \mathbf{V}^{(k)} \right\rangle = \delta_{j,k}, \quad (16)$$

to the Goldstone modes (7).

From (12), the Response Functions’ physical meaning is that a spiral wave is insensitive to small perturbations in the region where its RFs are close to zero. As experimental data [22] and computer simulations showed spiral waves’ insensitivity to distant events, it was conjectured [14] that the RFs must decay quickly with distance from the spiral wave core, *i.e.* spiral waves *look like* essentially non-localized objects but *behave* as effectively localized particles.

Note also that the RFs do not depend on time, *i.e.* are functions of the coordinates only, in the co-rotating system of reference. Thus, there is reduction in the description of the smooth dynamics of spiral waves from the system of nonlinear partial differential equations (1) to the system of ordinary differential equations (11) describing the movement of the core of the spiral and the shift of its angular velocity, if the spiral wave’s response functions are known explicitly. Not only is explicit knowledge of the response functions important, but it is necessary to confirm that on an unbounded medium they are sufficiently localized that the convolution integral in (12) converges.

To confirm the spirals’ “wave-particle duality” conjecture, the localized response functions were to be first found explicitly and then tried for *quantitative* prediction of the drift due to various small perturbations in a particular model medium. For the model *oscillatory medium* described by the Complex Ginzburg-Landau Equation, it has been demonstrated that the spiral wave response functions are localized, *i.e.* essentially differ from zero only in the very vicinity of the spiral wave core, for all sets of the model parameters stable spiral waves exist for [23–25]. Most importantly, the response functions have demonstrated the ability to make quantitative predictions of drift of spirals due to small perturbations of any nature [25–27].

Effective control of the spiral wave dynamics is of interest for numerous applications, *e.g.* control of re-entry in the

heart. Although some cardiac pathology had been attributed to autorhythmic activity which may be described in terms of oscillatory reaction-diffusion systems, much more important for cardiac applications is dynamics of spiral waves in *excitable* media, as most cardiac tissues are excitable. Attempts have been made to compute the response functions in Barkley [28, 29] and FitzHugh-Nagumo [30] models of excitable media. For the chosen parameters of the medium, the computed RFs appeared effectively localized in the vicinity of the spiral wave core. In [29], Hakim and Henry computed the response functions with the accuracy allowing quantitative description of deformations of scroll waves.

Encouraging as these results are, there is a need for proven robust method to compute accurately the response functions of spiral waves in a variety of excitable media. In this paper, we present such a method and demonstrate that it work for stationary rotating spirals in FitzHugh-Nagumo system. We demonstrate convergence of the method with respect to the computational parameters, *i.e.* discretization steps and size of the medium. The obtained Response Functions are localized at the spiral's core.

## II. METHODS

### A. Computations

To compute the response functions, we use methods similar to those described in [16, 21].

The nonlinear problem (3) is considered on a disk  $\rho \leq R$ , with homogeneous Neumann boundary conditions,  $\partial_\rho \mathbf{U}(R, \theta) = 0$ . The fields are discretized on a regular polar grid  $(\rho_j, \theta_k) = (j\Delta\rho, k\Delta\theta)$  where  $0 < j \leq N_\rho$  and  $0 \leq k < N_\theta$  plus the center point  $\rho = 0$ , hence there are  $N_\rho N_\theta + 1$  grid points and correspondingly  $N = \ell(N_\rho N_\theta + 1)$  unknowns and the same number of equations in discretization of (3). In the inner points  $j < N_\rho$ , the  $\rho$ -derivatives are calculated via second-order central differences. The  $\theta$ -derivatives are calculated using Fornberg's `weights.f` subroutine [31] which uses all  $N_\theta$  values so, in theory, provides an approximation of  $\theta$ -derivatives of the order of  $N_\theta$ . The discretization of the Laplacian at the center point is via the difference between the average through the innermost circle  $\rho = \Delta\rho$  and the center point, and approximation at  $j = N_\rho$  takes into account the boundary conditions at  $\rho = R$ .

The discretized nonlinear steady-state spiral problem (3) is solved by Newton method, starting from initial approximations obtained by interpolation of results of simulations of time-dependent problem (1) using EZSPIRAL. The Newton iterations involved inversion of the linearized matrix which has a banded structure with the bandwidth  $1 + 2\ell N_\theta$ ; this is achieved by appropriate ordering of the unknowns of the discretized problem within the  $N$ -dimensional vector of unknowns, so that the index enumerating components of reagent vectors from  $\mathbb{R}^\ell$  varied fastest, followed by the index enumerating angular grid points  $k\Delta\theta$ , followed by the index enumerating the radial grid points  $j\Delta\rho$ .

Thus posed discretized nonlinear problem inherits the

symmetry of (3) with respect to rotations. To select a unique solution out of a family of solutions generated by this symmetry, we impose a ‘‘pinning condition’’ of a form  $U_{\ell_*}(j_*\Delta\rho, k_*\Delta\theta) = u_*$ , where  $\ell_*$ ,  $u_*$  and  $j_*$  may be selected arbitrarily and  $k_*$  is chosen as the  $\theta$ -grid point in the  $\rho = j_*\Delta\rho$  circle that gives the  $\ell_*$ -component value closest to  $u_*$  in the initial approximation. Since  $U_{\ell_*}(j_*\Delta\rho, k_*\Delta\theta)$  is fixed, it is no longer an unknown, and its place in the  $\mathbb{R}^N$ -vector of unknowns is taken by  $\omega$ , also to be found from (3). In this way, the balance of the unknowns and equations is preserved. As  $\omega$  is present in all the equations, the corresponding non-zero column of the linearization matrix violated the bandedness of the matrix. This obstacle has been overcome by employing Sherman-Morrison formula [32] to find solutions of the corresponding linear systems using only banded matrices. Newton iterations are performed until the residual in the discretized equation (3) became sufficiently small.

The linearized problems (4) and (13) are considered in the same domain with similar boundary conditions. The critical eigenvalues and eigenvectors of the discretized operators  $\mathcal{L}$  and  $\mathcal{L}^+$  are computed with the help of a complex shift and Cayley transform.

For a matrix  $\mathbf{L}$ , be it discretization of  $\mathcal{L}$  or  $\mathcal{L}^+$ , the complex shift is defined as

$$\mathbf{A} = \mathbf{L} + i\kappa\mathbf{I}$$

and the subsequent Cayley transform as

$$\mathbf{B} = (\xi\mathbf{I} + \mathbf{A})^{-1}(\eta\mathbf{I} + \mathbf{A})$$

where  $\kappa$ ,  $\xi$  and  $\eta$  are real parameters and  $\mathbf{I}$  is the identity matrix. If  $\lambda$ ,  $\alpha$  and  $\beta$  are eigenvalues of respectively  $\mathbf{L}$ ,  $\mathbf{A}$  and  $\mathbf{B}$ , this implies

$$\alpha = \lambda + i\kappa, \quad \beta = \frac{\eta + \alpha}{\xi + \alpha}.$$

The selected eigenvalues and eigenvectors of thus constructed matrices  $\mathbf{B}$  are found using Arnoldi method, as implemented in ARPACK.

We have used  $\xi = 0$ ,  $\eta = 1$  and  $\kappa = 0, \mp\omega$  when looking, respectively, for  $\mathbf{V}^{(0, \pm 1)}$  and  $\mathbf{W}^{(0, \mp 1)}$ , where  $\omega$  is the solution of the corresponding nonlinear problem just obtained. With this choice of  $\xi$ ,  $\eta$  and  $\kappa$ , the numerical eigenvalues  $\hat{\lambda}$  and  $\hat{\mu}$  closest to the theoretical critical eigenvalues (6) and (14) correspondingly, generate the largest  $|\beta|$ . Hence, the Arnoldi method in each case is required to obtain the eigenvalue with the largest absolute value.

To normalize the eigenvectors, we use the ‘‘analytical’’ Goldstone modes  $\check{\mathbf{V}}^{(k)}$ , obtained by numerical differentiation of the numerical spiral wave solution  $\hat{\mathbf{U}}$ , namely,

$$\begin{aligned} \check{\mathbf{V}}^{(0)} &= -\partial_\theta \hat{\mathbf{U}}(\rho, \theta), \\ \check{\mathbf{V}}^{(\pm 1)} &= -\frac{1}{2} e^{\mp i\theta} (\partial_\rho \mp i\rho^{-1} \partial_\theta) \hat{\mathbf{U}}(\rho, \theta), \end{aligned}$$

where differentiation has been implemented using the same discretization schemes as used in calculations.

First, the response functions  $\hat{\mathbf{W}}^{(k)}$  computed by ARPACK are normalized with respect to the ‘‘analytical’’ Goldstone modes  $\check{\mathbf{V}}^{(k)}$  so that

$$\langle \hat{\mathbf{W}}^{(k)}, \check{\mathbf{V}}^{(k)} \rangle = 1, \quad k = 0, \pm 1,$$

where numerical integration involved in  $\langle \cdot, \cdot \rangle$  has been carried out using the trapezoidal rule.

Then, the computed by ARPACK ‘‘numerical’’ Goldstone modes  $\hat{\mathbf{V}}^{(k)}$  are normalized with respect to the normalized response functions so that

$$\langle \hat{\mathbf{W}}^{(k)}, \hat{\mathbf{V}}^{(k)} \rangle = 1, \quad k = 0, \pm 1.$$

Thus, we finally obtain

- a numerical solution for the spiral wave problem (3) together with the angular velocity  $\omega$ ,
- ‘‘analytical’’ Goldstone modes  $\check{\mathbf{V}}^{(k)}$ ,
- normalized ‘‘numerical’’ Goldstone modes  $\hat{\mathbf{V}}^{(k)}$ , and
- normalized Response Functions  $\hat{\mathbf{W}}^{(k)}$

### B. Analysis

To validate the computed Response Functions, we have to demonstrate convergence of the solution with respect to the numerical approximation parameters such as the size of the medium  $R$ , and discretization steps  $\Delta\rho$  and  $\Delta\theta$ .

First of all, we have to demonstrate convergence of the computed eigenvalues of  $\hat{\lambda}_n$  and  $\hat{\mu}_n$  to their theoretical values (6) and (14), taking for  $\omega$  its numerical approximation  $\hat{\omega}$  found by numerical solving the discretized problem (3). Since the ‘‘theoretical’’ value for  $\omega$  is not available, we can only check convergence of  $\hat{\omega}$  to some limit.

The accuracy of the ‘‘numerical’’ Goldstone modes is quantified by the distance between the ‘‘numerical’’ and ‘‘analytical’’ Goldstone modes, in  $L_2$  norm

$$\mathcal{D}_j = \left( \int_{\mathcal{S}} |\check{\mathbf{V}}^{(j)}(\vec{r}) - \hat{\mathbf{V}}^{(j)}(\vec{r})|^2 d^2\vec{r} \right)^{1/2}$$

as well as  $C_0$  norm

$$\mathcal{D}'_j = \max_{\vec{r} \in \mathcal{S}} |\check{\mathbf{V}}^{(j)}(\vec{r}) - \hat{\mathbf{V}}^{(j)}(\vec{r})|$$

over a disk  $\mathcal{S}$  of half the radius of the computational domain:

$$\mathcal{S} = \{\vec{r} : |\vec{r}| \leq R/2\}.$$

The smaller disk is used to exclude the effects of boundary conditions. The issue is that  $\check{\mathbf{V}}$  do not satisfy Neumann boundary conditions whereas  $\hat{\mathbf{V}}$  do, hence there is an inevitable deviation between them near  $\rho = R$ , which is an artefact of restricting our problem to a finite domain, and is

not indicative of accuracy of the found  $\hat{\mathbf{W}}$  which are expected to be exponentially small near  $\rho = R$ .

The accuracy of the computed response functions  $\hat{\mathbf{W}}$  could be tested directly in the same way as the accuracy of the computed  $\hat{\omega}$ , *i.e.* by the numerical convergence to some limit, or indirectly via the orthogonality between the response functions and the Goldstone modes required by (16). The direct test of the RFs convergence might be difficult to implement for the numerical solutions obtained on different meshes. Therefore, the convergence is checked indirectly via the orthogonality to the ‘‘analytical’’ GMs, quantified by

$$O_a = \sum_{j=0, \pm 1} \sum_{k=0, \pm 1} \left| \langle \hat{\mathbf{W}}^{(j)}, \check{\mathbf{V}}^{(k)} \rangle - \delta_{j,k} \right|^2$$

and orthogonality to the ‘‘numerical’’ GMs quantified by

$$O_n = \sum_{j=0, \pm 1} \sum_{k=0, \pm 1} \left| \langle \hat{\mathbf{W}}^{(j)}, \hat{\mathbf{V}}^{(k)} \rangle - \delta_{j,k} \right|^2.$$

Note, that by construction the diagonal elements of both the ‘‘numerical’’ and ‘‘analytical’’ biorthogonality matrices here are all equal to 1 up to round-off errors.

### III. RESULTS

We have tested our method for computing the response functions in the case of the FitzHugh-Nagumo model,  $\ell = 2$ ,

$$\begin{aligned} f_1 &= \varepsilon^{-1}(u_1 - u_1^3/3 - u_2), \\ f_2 &= \varepsilon(u_1 - au_2 + b), \end{aligned}$$

$\mathbf{D} = \begin{bmatrix} 1 & 0 \\ 0 & 0 \end{bmatrix}$ , with parameters  $a = 0.5$ ,  $b = 0.68$ ,  $\varepsilon = 0.3$ .

For pinning, we have used  $\ell_* = 2$ ,  $u_* = 0.1$  and  $j_* = N_\rho/2$ . Newton iterations have been performed until the Euclidean ( $l_2$ ) norm of the residual in the discretized nonlinear equation falls below  $10^{-8}$ . For comparison, we have also run cases, discussed later in fig. 5, in which iterations continue until the norm of the residual no longer decreases (typically such norms were below  $10^{-9}$  down to  $10^{-13}$ ). The tolerance in ARPACK’s routines `znaupd` and `zneupd` has been set to the default ‘‘machine epsilon’’. For the Krylov subspace dimensionality we have tried 3 and 10, with no perceptible difference in either the numerical results or the computation resources required.

Figures 1 and fig. 2 illustrate the spiral wave solution and the GMs and RFs for  $R = 25$ ,  $N_\rho = 1280$  and  $N_\theta = 64$ . This solution is taken as the best achievable given memory restrictions (4Gb of real memory). The angular velocity for it was found to be  $\hat{\omega} \approx 0.5819341748776017$ . For the GMs and RFs, shown are  $n = 0$  and  $n = 1$  modes only, since the calculated  $n = -1$  modes are very close to complex conjugates of the  $n = 1$  modes, which of course they should be.

One can see that the GMs  $\hat{\mathbf{V}}$  are indeed proportional to corresponding derivatives of the spiral wave solution  $\hat{\mathbf{U}}$ , and that



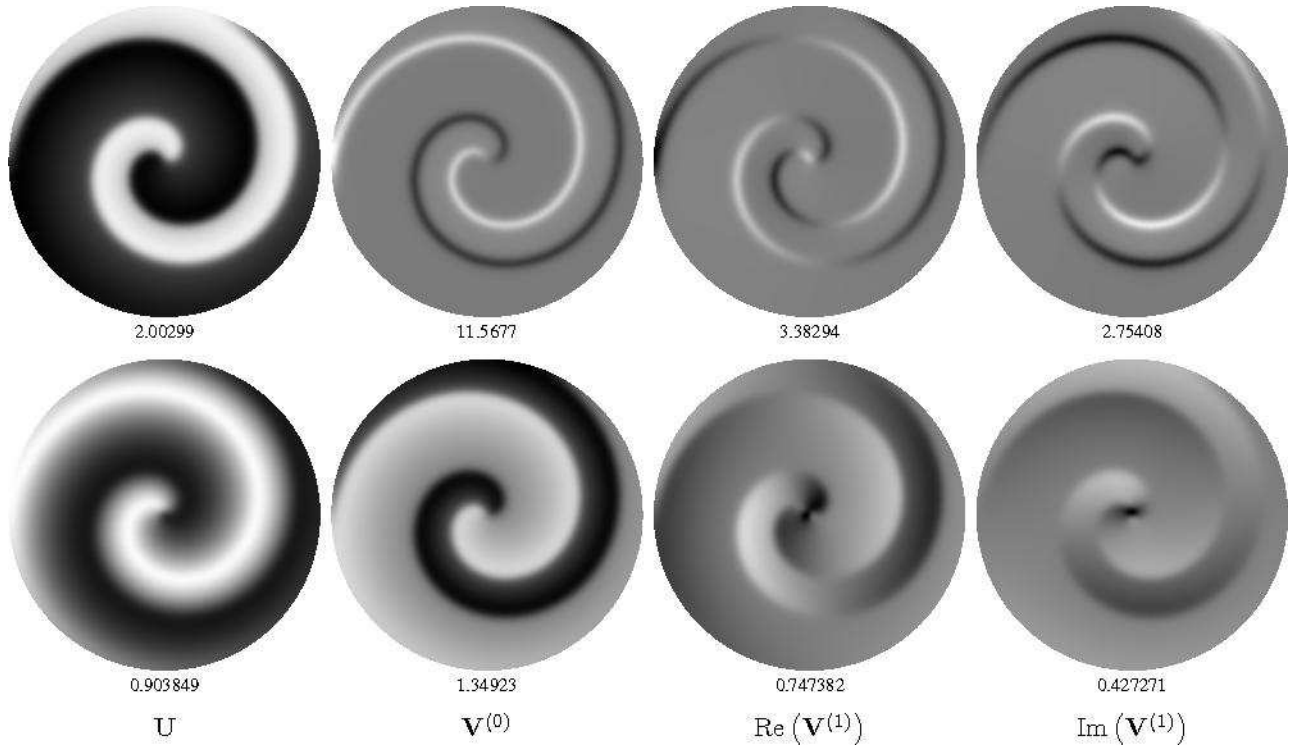


FIG. 1: Solutions of the nonlinear problem (3) and the linearized problem (4,5), *i.e.* the Goldstone modes, at the “best” parameters,  $R = 25$ ,  $N_\rho = 1280$ ,  $N_\theta = 64$ , as density plots. Numbers under the density plots are their amplitudes  $a$ : white of the plot corresponds to the value  $a$  and black corresponds to the value  $-a$  of the designated field. Upper row: 1st components, lower row: 2d components.

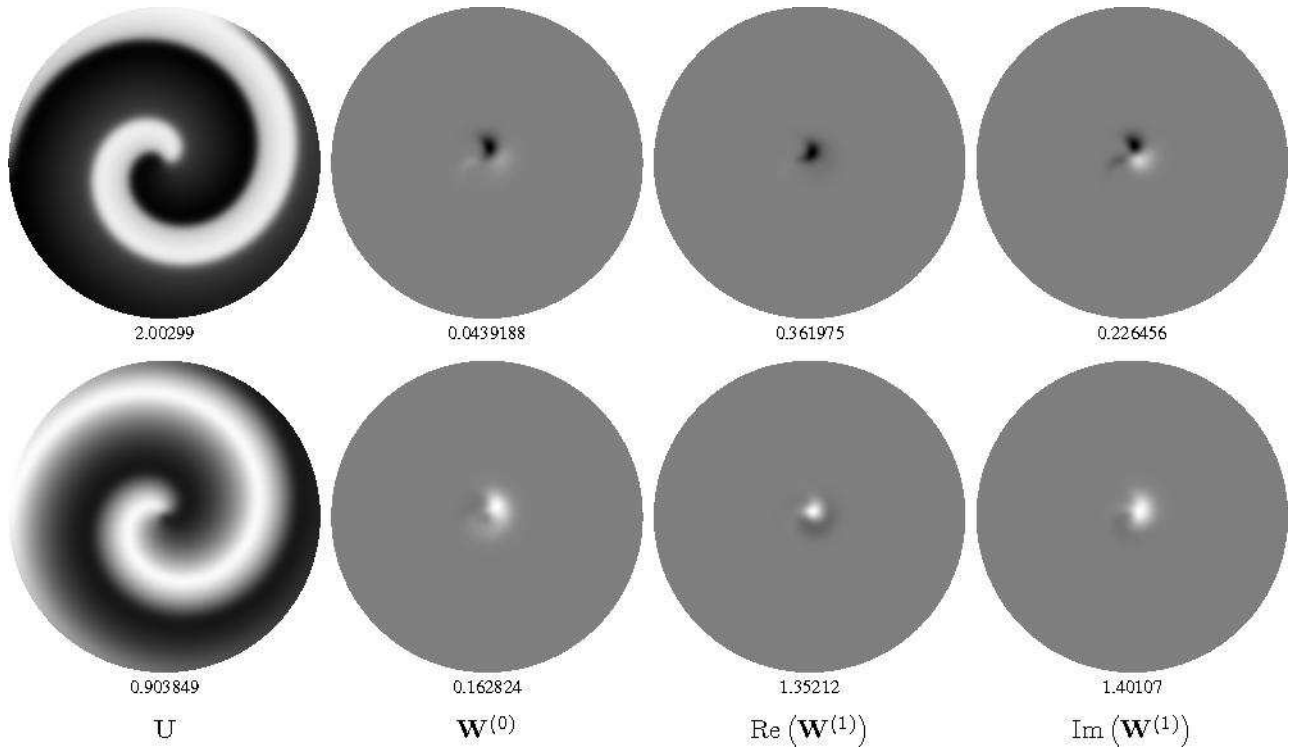


FIG. 2: Same visualization as in fig. 1, for the adjoint linearized problem (13,15), *i.e.* the response functions.

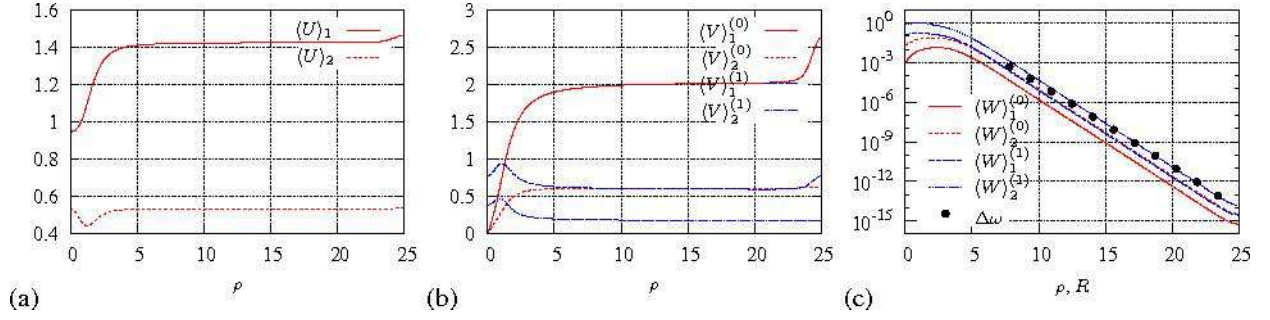


FIG. 3: Radial dependence of the angle-averaged solutions for the spiral wave (a), Goldstone modes (b) and response functions (c). In (c), the dependence of  $\Delta\omega(R) = \hat{\omega}(R) - \hat{\omega}(25)$  is shown for comparison, where  $\hat{\omega}(R)$  is the numerically found spiral angular velocity in the disk of given radius  $R$ .

the RFs  $\hat{W}$  are localized in a small region of the spiral tip and are indistinguishable from zero outside that region.

The character of the RFs' decay with distance is illustrated in more detail in fig. 3. There we depict the angle-averaged values of the solutions, defined as

$$\langle X \rangle_i^{(n)}(\rho) = \frac{1}{2\pi} \oint \hat{X}_i^{(n)}(\rho, \theta) d\theta,$$

for  $X = U, V$  and  $W$ . Note the contrast of the behavior of  $\langle U \rangle_i^{(n)}$  and  $\langle V \rangle_i^{(n)}$  on one hand and  $\langle W \rangle_i^{(n)}$  on the other hand. In the semilogarithmic coordinates of fig. 3(c) the graphs of  $\langle W \rangle_i^{(n)}(\rho)$  have straight shape for a large range of  $\rho$ , not too close to 0 or  $R = 25$ , and for several decades of magnitude of  $\langle W \rangle_i^{(n)}$ . This is an evidence of the expected exponential character of decay. For comparison, we also show convergence of  $\hat{\omega} = \hat{\omega}(R)$  in a disk as a function of the disk radius  $R$ . The general theory [24, 33–35] predicts that the  $\langle W \rangle_i^{(n)}(\rho)$  and  $\Delta\omega(R) = \hat{\omega}(R) - \hat{\omega}(\infty)$  dependencies should both be exponential decays with the same characteristic exponential; this agrees well with the numerical results shown in fig. 3(c).

The convergence of the method has been tested by changing one of the three numerical approximation parameters  $R$ ,  $N_\rho$  and  $N_\theta$  while keeping the other two at fixed values as in the “best example”. More specifically, while changing  $R$ , we considered two variants: with fixed  $N_\theta$ , and with changing  $N_\theta$  so that the combination  $R\Delta\theta$ , which is the size of the outermost computational cells in the angular direction, remained constant.

Fig. 4 illustrates the results of the study, where the four columns correspond to different series of calculations, and the three rows correspond to the three different methods of assessing the accuracy: closeness of the eigenvalues to the theoretical values, distance between “numerical” and “analytical” GMs and orthogonality between non-dual RFs and GMs. The scales of  $\Delta\rho$ ,  $\Delta\theta$  and the error estimates are logarithmic, and the scales of  $R$  are linear. Here shown is the distance between the “numerical” and “analytical” Goldstone modes in  $L_2$  norm, the distance in  $C_0$  norm looks similar.

A typical feature on many of the curves is a “knee”-shape, when the measure of the error decreases as  $R$  grows or  $\Delta\theta$  or  $\Delta\rho$  decrease, but only until a certain point, beyond which it reaches a plateau. This behavior is expected and explicable.

The calculation error is affected by many factors, and if the factor varied in a particular series becomes negligible, then the error remains at a constant level determined by fixed values of other factors.

The position of the “knees” on the curves indicates that the accuracy of the rotational ( $n = 0$ ) modes would be improved if  $\Delta\theta$  were further decreased (there are no knees on the curves corresponding to the rotational modes, red online, in the fourth, *i.e.* rightmost column), whereas the limiting parameter for the translational ( $n = 1$ ) modes is  $\Delta\rho$  (there is no knees on the curves corresponding to the translational modes, blue online, in the third column). The analysis of the first two columns is more complicated. The error estimates at the maximal  $R$  are similar in both columns as they correspond to the same “best” spiral. These limit values are achieved, *i.e.* plateaux are observed, at much smaller  $R$  values if  $\Delta\theta = \text{const}$ , than if  $R\Delta\theta = \text{const}$ . This is because reduction of  $R$  at fixed  $\Delta\theta$  produces an additional improvement of approximation due to the angular discretization. When  $R\Delta\theta$  is kept fixed, as in the first column, the dependence of the solution on the disk radius is without this extra benefit.

The rates of convergence with respect to parameters can be assessed by the slopes of the curves above the knees before they plateau. In some cases the data is somewhat irregular, primarily at parameters corresponding to lower values of error estimates. This is not unexpected and we attribute it to incomplete convergence of the iterative procedures (see below). On the whole the slopes can be determined clearly from these plots.

The constant slope in the first (leftmost) and the second columns corresponds to the exponential convergence with  $R$ . The constant slope in the third column corresponds to the power convergence, and the typical slope there is 2. This is well seen on the curves for translational modes, blue online, and not well on the curves for rotational modes, red online, which are very small anyway. Slope 2 is of course what should be expected as our discretization is second-order in  $\Delta\rho$  in all cases. The curves in the fourth (rightmost) column are convex, which is consistent with the fact that the order of approximation is  $N_\theta$  which varies along the curve as  $\Delta\theta$  values, since  $N_\theta = 2\pi/\Delta\theta$ , so the slope is bigger for smaller  $\Delta\theta$ . Note also that the convergence in  $\Delta\theta$  is very fast, which is consis-

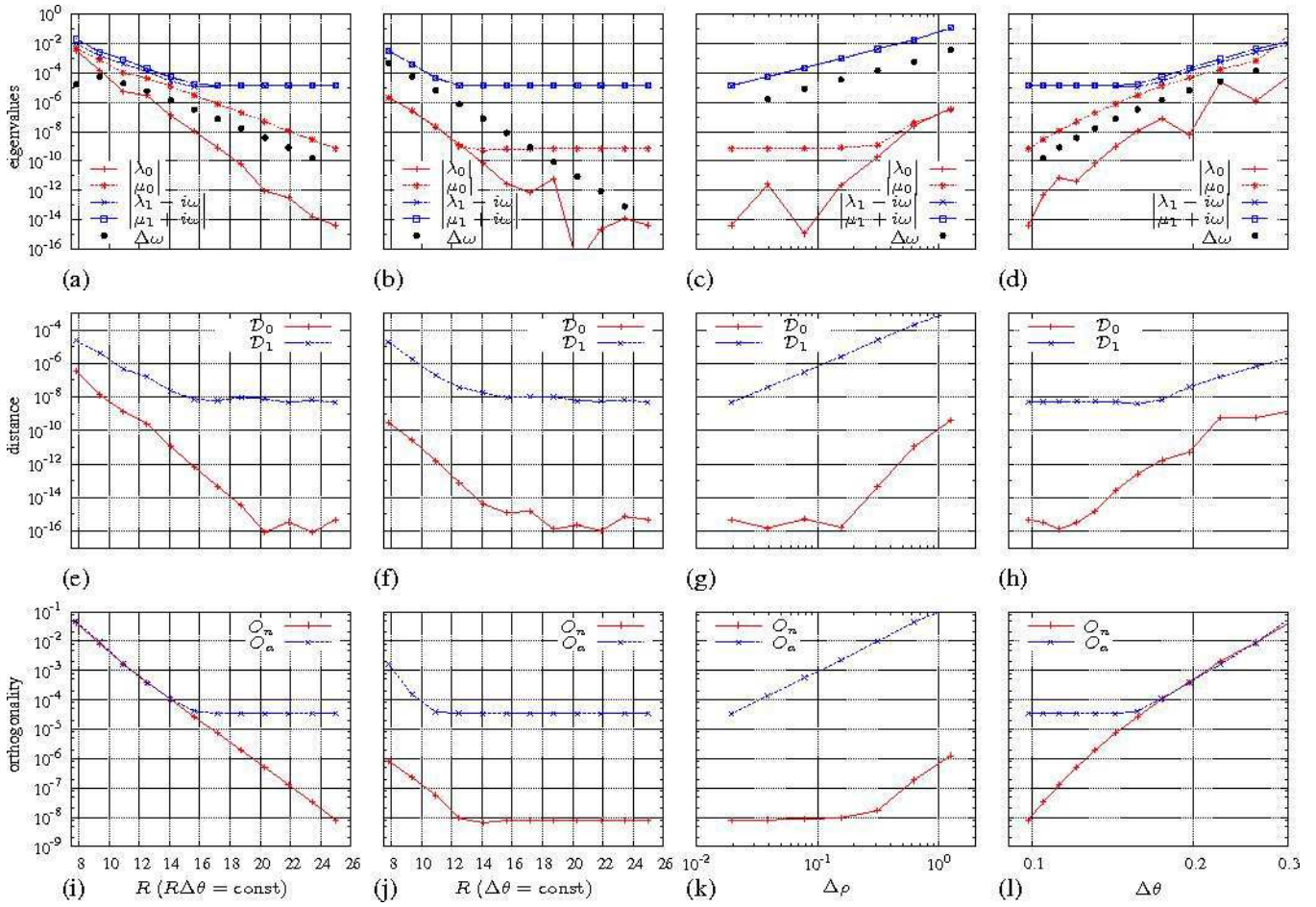


FIG. 4: Convergence in numerical parameters: of deviation of the numerical eigenvalues from theoretical (upper row), of  $L_2$  distance between numerical and theoretical eigenfunctions (second row) and of orthogonality, *i.e.* Frobenius norm of the difference of the matrix of scalar products of eigenfunctions and adjoint eigenfunctions from the unity matrix (third row), as dependencies of disk radius (first and second columns), radius discretization step (third column) and polar angle discretization step (fourth column). In the first column,  $R$  is changed with the value of  $\Delta\rho$  and  $R\Delta\theta$  constant. In the second column,  $R$  is changed with  $\Delta\rho$  and  $\Delta\theta$  constant.

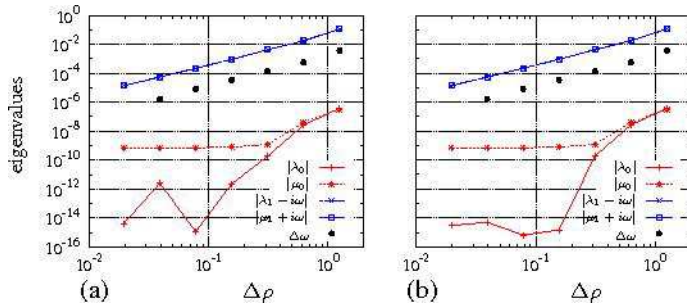


FIG. 5: Effect of the accuracy of the unperturbed spiral wave solution on the convergence. (a) Newton iteration tolerance  $10^{-8}$ . (b) Newton iterations until the norm of the residual stopped decreasing.

tent with the high-order of the Fornberg approximation of the  $\theta$  derivatives.

Finally, the irregular shape of some of the curves in fig. 4 at very low values of error estimates is related to the accuracy of finding the spiral solution and is in fact affected by the

processor precision. Note that all calculations in fig. 4 have been performed with Newton iterations tolerance of  $10^{-8}$ , and some of the curves fall down as low as  $10^{-15}$  *i.e.* close to the machine epsilon. A change in the Newton iteration tolerance affects the curves at those low values, as shown in fig. 5.

#### IV. CONCLUSIONS

We have presented a general, robust method for obtaining Response Functions for spiral waves in excitable media. We have assessed the method in the case of rigidly rotating spiral waves and we have studied the convergence of the spiral wave and the eigenfunctions, both the Goldstone Modes and the Response Functions, with respect to the numerical approximation parameters  $R$ ,  $N_\rho$  and  $N_\theta$ . The rates of convergence are found to agree with the order of approximation and indicate the accuracy with which solutions can be found for particular numerical parameters.

The computed Response Functions are localized in the



vicinity of the spiral wave tip and exponentially decay with distance from it. This localization ensures convergence of the convolution integral in (12) in an unbounded domain.

The eigenvectors of the linearized operator, *i.e.* Goldstone modes and of its adjoint, *i.e.* the Response Functions have been computed using the same technique, so the qualitatively different behavior of these solutions at large  $r$  is not a numerical artefact, as it was not in any way assumed in the numerical method.

Although the method has been used here to compute the response functions in the FitzHugh-Nagumo model, the method is independent of the particular reaction kinetics and should be widely applicable to the computation of Response Functions

of rigidly rotating waves in any other model of excitable tissue. Moreover, the method can also be extended in a straightforward way to include additional effects, such as the effect of uniform twist along scroll waves with linear filaments in three dimensions [17, 29, 36].

### Acknowledgement

This study has been supported in part by EPSRC grant EP/D074789/1.

- 
- [1] T. Frisch, S. Rica, P. Coulet, and J. M. Gilli, *Phys. Rev. Lett.* **72**, 1471 (1994).
- [2] D. J. Yu, W. P. Lu, and R. G. Harrison, *Journal of Optics B — Quantum and Semiclassical Optics* **1**, 25 (1999).
- [3] B. F. Madore and W. L. Freedman, *Am. Sci.* **75**, 252 (1987).
- [4] L. S. Schulman and P. E. Seiden, *Science* **233**, 425 (1986).
- [5] A. M. Zhabotinsky and A. N. Zaikin, in *Oscillatory processes in biological and chemical systems*, edited by E. E. Selkov, A. A. Zhabotinsky, and S. E. Shnol (Nauka, Pushchino, 1971), p. 279, in Russian.
- [6] S. Jakubith, H. H. Rotermund, W. Engel, A. von Oertzen, and G. Ertl, *Phys. Rev. Lett.* **65**, 3013 (1990).
- [7] K. Agladze and O. Steinbock, *J.Phys.Chem. A* **104** (44), 9816 (2000).
- [8] M. A. Allesie, F. I. M. Bonk, and F. Schopman, *Circ. Res.* **33**, 54 (1973).
- [9] N. A. Gorelova and J. Bures, *J. Neurobiol.* **14**, 353 (1983).
- [10] F. Alcantara and M. Monk, *J. Gen. Microbiol.* **85**, 321 (1974).
- [11] J. Lechleiter, S. Girard, E. Peralta, and D. Clapham, *Science* **252** (1991).
- [12] A. B. Carey, R. H. Giles, Jr., and R. G. Mclean, *Am. J. Trop. Med. Hyg.* **27**, 573 (1978).
- [13] J. D. Murray, E. A. Stanley, and D. L. Brown, *Proc. Roy. Soc. Lond. ser. B* **229**, 111 (1986).
- [14] V. N. Biktashev, Ph.D. thesis, MPhTI (1989), in Russian.
- [15] V. Biktashev and A. Holden, *Chaos, Solitons and Fractals* **5**, 575 (1995).
- [16] D. Barkley, *Phys. Rev. Lett.* **68**, 2090 (1992).
- [17] V. N. Biktashev, *Physica D* **36**, 167 (1989).
- [18] B. Sandstede and A. Scheel, *Physica D* pp. 233–277 (2000).
- [19] B. Sandstede and A. Scheel, *Phys. Rev. E* pp. 7708–7714 (2000).
- [20] B. Sandstede and A. Scheel, *Phys. Rev. Lett.* **86**, 171 (2001).
- [21] P. Wheeler and D. Barkley, *SIAM Journal on Applied Dynamical Systems* **5**(1), 157 (2006).
- [22] K. I. Agladze, private communication (2000).
- [23] I. V. Biktasheva, Y. E. Elkin, and V. N. Biktashev, *Phys. Rev. E* **57**, 2656 (1998).
- [24] I. V. Biktasheva and V. N. Biktashev, *J. Nonlin. Math. Phys.* **8 Supl.**, 28 (2001).
- [25] I. V. Biktasheva and V. N. Biktashev, *Phys. Rev. E* **67**, 026221 (2003).
- [26] I. V. Biktasheva, Y. E. Elkin, and V. N. Biktashev, *J. Biol. Phys.* **25**, 115 (1999).
- [27] I. V. Biktasheva, *Phys. Rev. E* **62**, 8800 (2000).
- [28] E. Hamm, Ph.D. thesis, Université de Nice - Sophia Antipolice / Institut Non Linéair de Nice (1997), french.
- [29] H. Henry and V. Hakim, *Phys. Rev. E* **65**, 046235 (2002).
- [30] I. V. Biktasheva, A. V. Holden, and V. N. Biktashev, *IJBC* **16**, 1547 (2006).
- [31] B. Fornberg, *A Practical Guide to Pseudospectral Methods* (Cambridge University Press, 1998).
- [32] W. Press, B. Flannery, S. Teukolsky, and W. Vetterling, *Numerical Recipes in C* (Cambridge University Press, Cambridge, UK, 1992).
- [33] P. S. Hagan, *SIAM J. Appl. Math.* **42**, 762 (1982).
- [34] V. N. Biktashev, in *Nonlinear Waves II. Dynamics and evolution*, edited by A. V. Gaponov-Grekhov, M. I. Rabinovich, and J. Engelbrecht (Springer, Berlin, 1989), pp. 87–96.
- [35] B. Sandstede, private communication (2005).
- [36] D. Margerit and D. Barkley, *Phys. Rev. Lett.* **86**, 175 (2001).